Nanocrystalline Manganese Substituted Nickel Ferrite Thick Films as PPM Level H_2S Gas Sensors

R. S. Pandav, A. S. Tapase, P. P. Hankare
Department of Chemistry,
Shivaji University, Kolhapur,
MHS, 416 004, India
E-mail: p_hankarep@rediffmail.com

G. B. Shelke, D. R. Patil*
Bulk and Nanomaterials Research Lab.,
Dept. of Physics, R. L. College, Parola,
Dist. Jalgaon, MHS, India, 425111
**E-mail: prof_drpatil@yahoo.in Mob: +91 9860335029*

Abstract- A simple sol-gel auto combustion technique is introduced for the synthesis of nanocrystalline manganese substituted nickel ferrite dry powders. These dry powders were mechano-chemically mixed with organic binders to prepare thixotropic pastes. Thixotropic pastes of as prepared ferrite powders were formulated and screen printed on glass substrates to form thick films, followed by firing at 450^{o}C. The crystal structure, phase, surface morphology and topography of the samples were characterized by X-ray diffraction study, scanning electron microscopy, transmission electron microscopy, etc. The gas sensing behavior of the samples were characterized by exposing the films to various inflammable and toxic gases like LPG, NH_3, CO_2, ethanol, H_2S and Cl_2. It was found that the sensors made from the composition containing x=1.0, exhibits highly selective and most sensitive towards 20 ppm of H_2S gas at 350^{0}C. The effect of operating temperature, gas concentration, type of gases, etc. on gas response were studied and discussed.

Keywords: *Sol-gel, Ferrites, H_2S gas sensors, etc.*

*****

I. INTRODUCTION

Various polluting, toxic and hazardous gases have been liberated by the industries, which can cause the disastrous and defective deformation of living beings, even at trace levels. This is attributed to explosive industrialization, modernization, globalization, urbanization, and what not? In past decades sensors were based on semiconductor metal oxides like SnO_2, ZnO, WO_3, etc. Spinel oxides (AB_2O_4) have been known for a long time for their interesting optical, electronic and magnetic properties and are thus suitable for various industrial applications, viz. magnetic cores, high-frequency devices, etc. Nowadays, spinel oxides show their characteristic response towards various gases [1-10]. Many researchers synthesized ferrites and worked for the study of their gas sensing properties [11-12].

Also, H_2S is highly toxic and hazardous in such a way that, the few minute exposure to 1000 ppm concentration in air can be fatal to human, high doses can produce unconsciousness and respiratory paralysis. Thus monitoring and control of H_2S gas is today's need. Semiconducting oxides, mixed oxides, spinel oxides, ZnO, CuO/SnO_2 composites, chemically modified $CdIn_2O_4$ thick films, surface modified Cr_2O_3, WO_3, etc. are studied for H_2S gas sensor [13-19]. However selectivity remains the main challenge for such materials. Hence there always needs for improved H_2S sensor in the industrial area, which has high gas response, high selectivity, low response time and low recovery time along with long term stability. It is known that the electrical resistivity of a semiconducting oxide can be modified by adsorption of gases [20]. This property has been used in semiconductor sensors for the detection of inflammable and toxic gases [21-23]. The semiconductor gas sensors offer good advantages with respect to other gas sensor devices due to their lowest cost, high applicability, high reliability, affordable to laymen, real-time control systems, etc. [24]. In recent years the ferrites have demonstrated to be good materials for gas sensing applications [25].

The efforts are made to synthesize the nanoscaled ferrite material by sol-gel technique, one of the most suitable, simple, easily available and low cost techniques for the synthesis of Mn substituted Nickel Ferrite.

II. EXPERIMENTAL TECHNIQUES

A. Synthesis of $NiFe_{2-x}Mn_xO_4$ compositions

High purity AR grade ferric nitrate, manganese nitrate, nickel nitrate and citric acid were used in the synthesis. The metal nitrate solutions were mixed in the required stiochiometric ratios in deionized water. The pH of the solution was adjusted in the range from 9.1 to 9.5 by adding ammonia solution, drop wise and slowly. The solution was allowed for slow heating around 373^{o}K with constant stirring, to obtain floppy mass, which was further subjected to thermal analysis for phase temperature identification. Thus, powdered samples of $NiFe_{2-x}Mn_xO_4$, ($0.0 \leq x \leq 2.0$) for various concentrations of Fe and Mn were synthesized by sol-gel auto-combustion method. Thick films of as prepared samples were fabricated by screen printing technique [26-27].

III. CHARACTERIZATION TECHNIQUES

A. X-Ray Diffraction Studies (XRD)

X-ray diffraction patterns of Mn-substituted nickel ferrites are shown in Fig.1. From Table 1, it is showed that, all the samples of system are cubic and the lattice constant increases with substitution of manganese content. The increase in lattice constant with increase in Mn content is due to the higher ionic radii of Mn^{3+} (0.65Å) ions as compared to Fe^{3+} (0.64Å) ions. Here Mn has strong site preference energy for octahedral site; it tends to occupy the B site rather than A-site. From the X-ray diffraction peaks,

 ISSN: 2321-8169
5152 - 5156

average crystallite size can be estimated using Debye-Scherer's formula.

$$t = 0.9\lambda / \beta \cos\theta \quad (1)$$

The X-ray density (dx) was calculated using the following relation.

$$dx = 8M/Na^3 \quad (2)$$

Where, N = Avagadros number (6.023 x 10^{23} atom/mole)
M = Molecular weight in gm
a = Lattice constant

The values of lattice constant (a), crystallite size (t) and X-ray density (dx) are summarized in Table.1. The values of interplanner spacing (d), hkl planes and lattice constant (*a*) were obtained from XRD data with an accuracy of ±0.03Å.

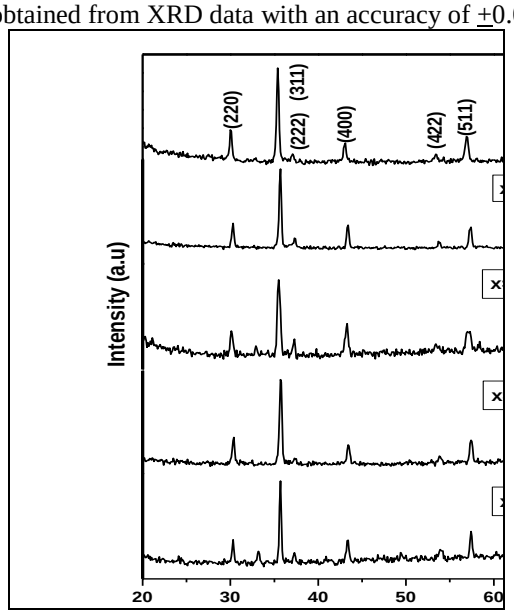

Fig.1: XRD of $NiFe_{2-x}Mn_xO_4$ system

Dopant Concentration (x)	Lattice Constant 'a' (Å)	X-ray density (gm/cm^3)	Crystallite size (nm)
0.0	8.33	5.37	31
0.5	8.34	5.34	28
1.0	8.35	5.31	24
1.5	8.37	5.26	28
2.0	8.38	5.22	27

Table 1: Lattice constant, crystallite size and X-ray density for all compositions

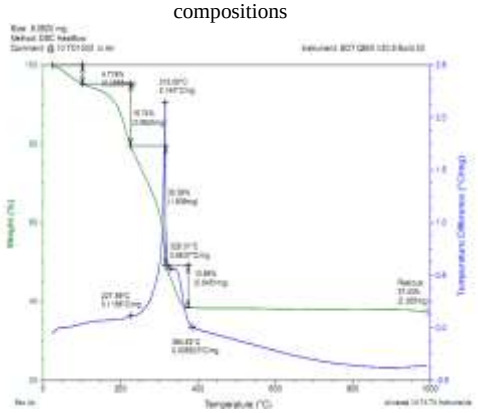

Fig.2: TGA-DTA traces for the sample for x = 1.0

B. Thermal Analysis (TGA and DTA)

Thermogravimetric analysis (TGA) and differential thermal analysis (DTA) of the precursor with x = 1.0 was carried out from room temperature to 1000°C to determine its decomposition behavior (Fig. 2). Sample powders of about 6 mg were placed in a platinum crucible, ignited alumina was used as the reference material with the heating rate of $10^oC \cdot min^{-1}$. The thermal analyses were carried out in static air and some thermoanalytical curves were recorded [27]. TGA of the precursor shows about 50% weight loss during this heating which is due to liberation of CO_2, H_2O, NO_x, etc. It was found that all the decomposition occurs at or below 400°C. Above which, the precursor exhibits a near about constant weight.

C. Microstructural Studies (SEM and TEM)

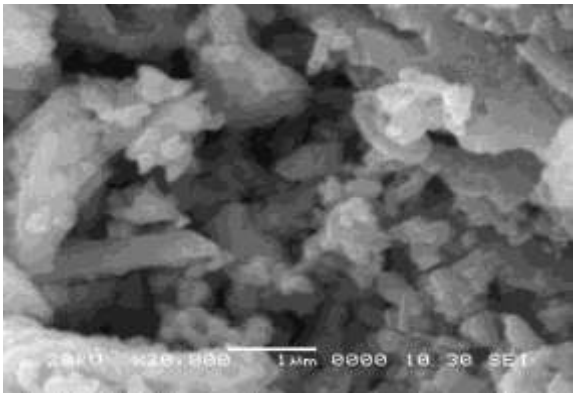

(a) x = 0.0

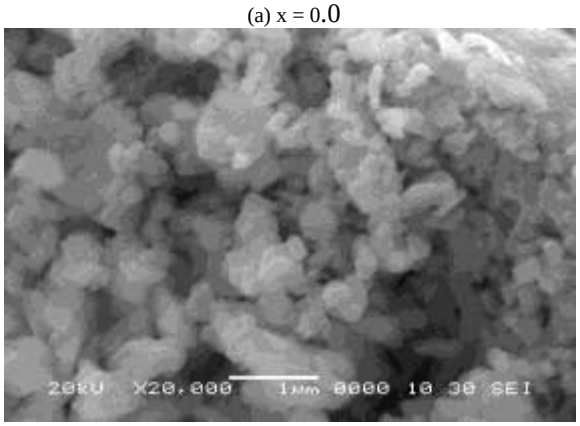

(b) x = 1.0

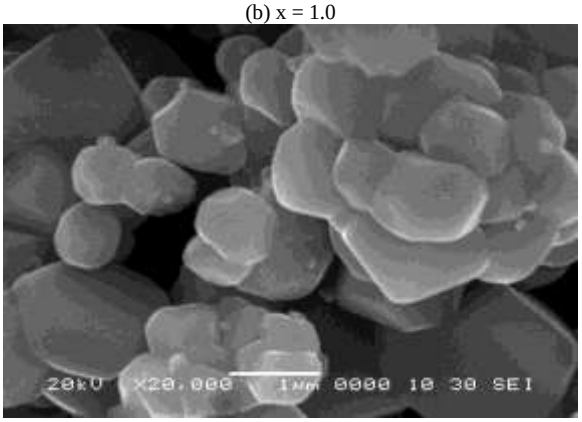

(C) x = 2.0

Fig. 3 SEM images of $NiFe_{2-x}Mn_xO_4$ system

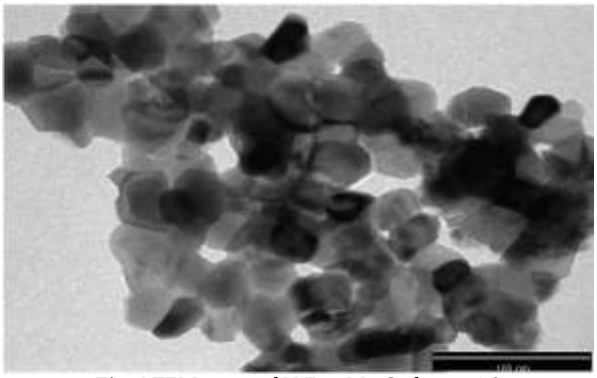

Fig. 4 TEM image of $NiFe_{2-x}Mn_xO_4$ for x = 1.0

The SEM images of Mn substituted nickel ferrites are shown in Fig.3. It is observed that, the average grain size goes on increasing on substitution of Mn content. They show the presence of very large lumps and found to be agglomeration of small spherical particles. This can be attributed to the generation of large volume of gases during the combustion reaction which occurs in a very short time. The morphology and grain size of manganese substituted nickel ferrite powder (where x=1) was further studied by TEM (Fig. 4). In manganese substituted nickel ferrite, it is noted that all particles are uniform and the average grain size is ~50 nm. Selected area electron diffraction pattern (SAED) of the particles suggests the polycrystallinity of individual crystallite and also confirms the formation of spinel ferrites.

D. Electrical behavior of the sample (Resistivity)

The d.c. electrical resistivity measurements showed linear plots of log (ρ) vs 1000/T°K up to 400°C without any break or inflexion. Silver paste is applied at both the ends of the films for proper contact and connections. The results of electrical measurements show the decrease in resistivity with increasing temperature (Fig. 5) proving the negative temperature coefficient of resistance for the samples to be studied. Increase in temperature of the sample will help the trapped charges to be liberated and participate in the conduction process, with the result of decrease in the resistivity. The electrical resistivity temperature behavior of the $NiFe_{2-x}Mn_xO_4$ system was found to be obeying Wilson's law [28].

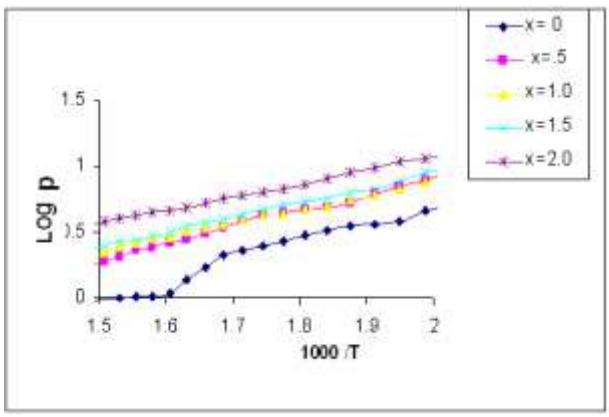

Fig. 5 log ρ versus 1000 / T°K for the sample $NiFe_{2-x}Mn_xO_4$

IV. GAS SENSING

Sensing parameters for gas sensors viz. gas response, selectivity, response time and recovery time, are defined elsewhere [28-36]. Various parameters affect the gas sensing behavior of the sensor. Their effects are discussed below.

A. Effect of Operating Temperature

Fig. 6 depicts the gas responses of $NiFe_{2-x}Mn_xO_4$ compositions with different operating temperatures. The $NiFe_{2-x}Mn_xO_4$ film for x = 1.0 was observed to be a most sensitive film and shows maximum response to 20 ppm H_2S gas at 350°C. The maximum response of this film is attributed to the fact that, it adsorbs more oxygen species on the surface at such a higher temperature (350°C). Upon exposure, the H_2S gas gets oxidized with adsorbed oxygen species on the surface of the film, trapping behind the electrons in the conduction band, which results in increase in conductance of the sensor. Thus this sensor monitors H_2S gas in the open environment.

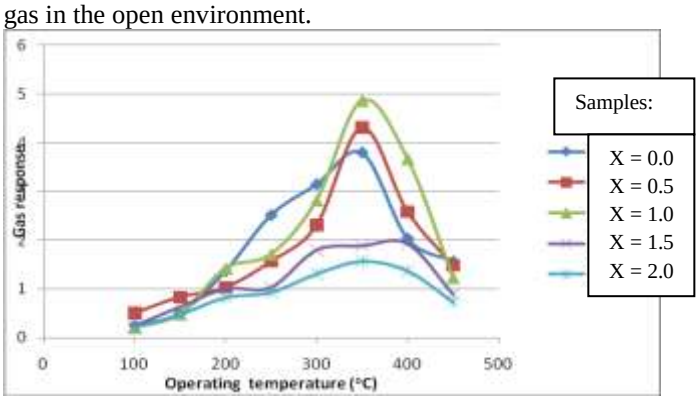

Fig. 6 Variation of gas response with op. temperature

B. Effect of H_2S Gas Concentration

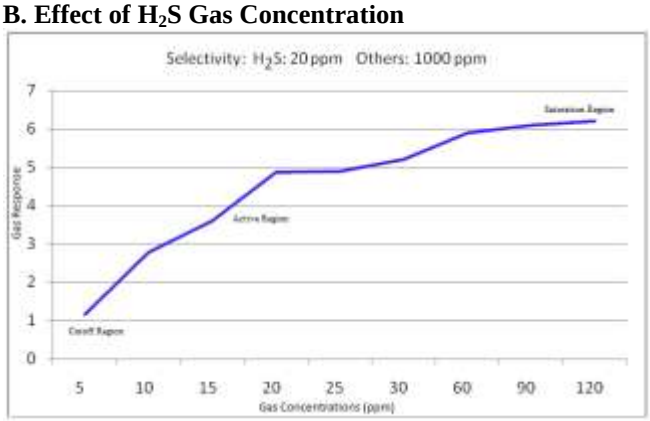

Fig. 7 Variation in gas response with gas concentration (ppm)

Fig. 7 depicts the variation of gas response of sample with H_2S gas concentration at 350°C operating temperature. The sensor was exposed to the varying concentrations of H_2S gas at higher temperature (350°C). The gas response was observed to increase linearly with the gas concentration up to 20 ppm. The increasing rate of gas response was relatively larger upto 20 ppm, and smaller afterwards. The region below 10 ppm, is called as cutoff region. The region in between 10 to 20 ppm is called as active region and above

 ISSN: 2321-8169
5152 - 5156

20 ppm, a saturation region. For the sensors to work proper, the sensor should work in the active region.

C. Selective Nature of the Sensor

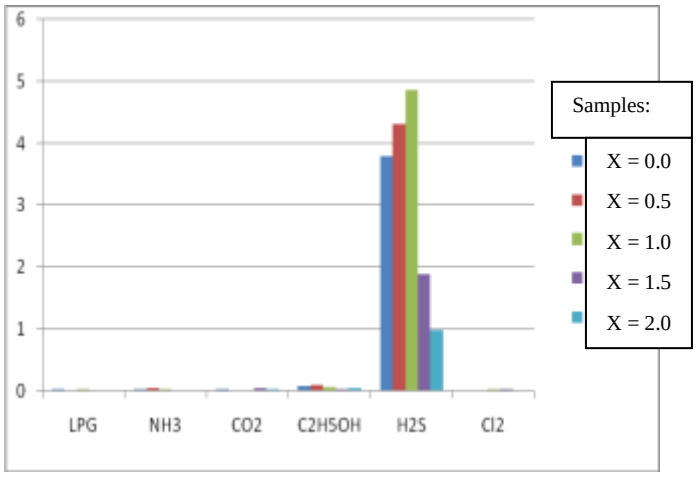

Fig. 8 Selectivity to H_2S gas among various gases

The selective nature of the sensor to H_2S gas at 350^oC is depicted in Fig. 8. The sensor showed high selectivity to H_2S against LPG, CO_2, C_2H_5OH, NH_3, and Cl_2 gases even at higher gas concentrations (1000 ppm).

V. DISCUSSION

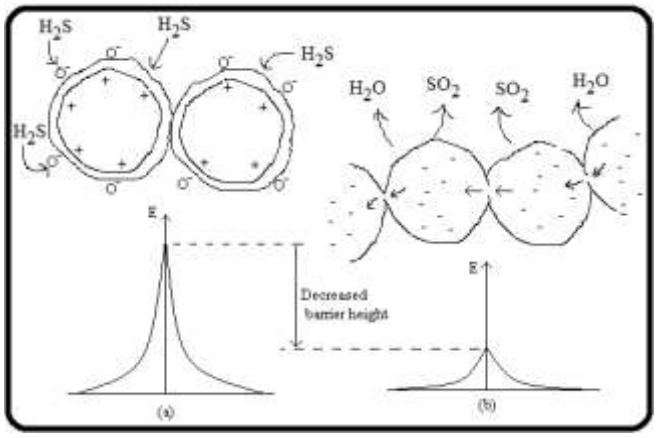

Fig. 9 Actual sensing mechanism to H_2S gas

Gas sensing (Fig. 9) is the surface phenomenon. However, the surface is the region where periodicity of the crystal is interrupted, which leads the formation of localized energy levels, in the forbidden gap. Such energy levels can either capture electrons or donate electrons. Such energy levels are completely ionized at higher temperature, causing the increase in conductance of the sensor.

The selective response of this sensor to ppm level H_2S gas at higher temperature could be attributed to the adsorption-desorption type of sensing mechanism. At higher temperature (~350^oC), more oxygen species (O^-) are adsorbed on the surface of the sensor. Upon exposure, the H_2S gas gets oxidized with the adsorbed oxygen species viz. ($O_2^- \rightarrow 2O^- \rightarrow O^{2-}$). The oxygen adsorption on the surface of the sensor occurs at different temperature ranges [13] are as follows:

$$O_{2\,(RT)} \xrightarrow{\text{upto } 150^0C} O_2^- \xrightarrow{\text{upto } 450^0C} 2O^- \xrightarrow{\text{Above } 450^0C} O^{-2}$$

During oxidation of the gas, the electrons are released soon and become free to carry the current.

$$2\,H_2S + 3O_{2\,(350^oC)} (\longrightarrow 6\,O^-) \rightarrow 2\,SO_2 + 2\,H_2O + 6\,e^-$$

At lower temperature, the smaller amount of oxygen would be adsorbed causes least oxidation of target gas, resulting in smaller gas response. At higher temperature (> 350^0C), the target gas may be oxidized before reaching the surface. Therefore, the gas response decreases further with increasing temperature.

This shows n-type conduction mechanism. Thus generated electrons contribute to sudden increase in conductance of the thick film. On exposure to the H_2S containing atmosphere, the resistance was observed to decrease crucially. Thus, obtains good response to 20 ppm H_2S gas. As SO_2 and water vapors are released from the film surface, the sensor recovers back to its original chemical status which would result in fast recovery.

VI. CONCLUSION

Manganese substituted nickel ferrites of nanocrystalline nature were successfully synthesized by sol-gel auto-combustion method. All the synthesized ferrospinel samples are in nanocrystalline (~50nm) form. Sensor having equivalent amount of Fe and Mn ions (x=1) shows higher response and better selectivity to H_2S gas.

ACKNOWLEDGEMENTS

Authors are grateful to Hon'ble Kakasaheb Vasantrao More, President and Prin. B. V. Patil, Rani Laxmibai Mahavidyalaya, Parola, Jalgaon, MHS, India for providing excellent laboratory facilities, at Bulk and Nanomaterials Research Laboratory. PPH thankful to UGC for BSR fellowship and RSP is very thankful to UGC, New Delhi for financial assistance through Rajiv Gandhi National Fellowship.

REFERENCES

[1]. K. K. Khun, A. Mahajan and R. K. Bedi, J. Appl. Phys. 106, (2009).
[2]. Wen Zeng , Tianmo Liu and Zhongchang Wang, J. Mater. Chem., 22, (2012), 3544-3548.
[3]. Young-Jin Choi, In-Sung Hwang, Jae-Gwan Park, Nanotechnology 19, (2008), 095508.
[4]. Shudi Peng, Gaolin Wu, Wei Song, and Qian Wang, J. Nanomater. (2013), Article ID 135147.
[5]. A. V. Zaytseva, V. B. Zaytsev M. N. Rumyantseva, A. M. Gaskov, A. A. Zhukova, J. Nanoelectronics and Optoelectronics, 7, (2012), 607-613.
[6]. T. SicilianoA. Tepore, G. Micocci, A. Serra, D. Manno, E. Filippo, Sens. Actuators B 133, 1, (2008), 321–326
[7]. S. Piperno, M. Passacantando, S. Santucci, L. Lozzi, and S. La Rosa, J. Appl. Phys. 101, (2007) 124504.

[8]. P. Misra, R. K. Shukla, L. M. Bali, G. C. Dubey, Sens. Actuators B 02 (2013) 210-215.
[9]. J. J. Vijaya , L. J. Kennedy , G. Sekaran, R. Thinesh Kumar ,P. Amalthi, K.S. Nagaraja, Sens. Actuators B 129 (2008) 741–749.
[10]. J. Judith Vijaya, L. John Kennedy, G. Sekaran, K.S. Nagaraja, Material Letters 61 (2007) 5213–5216.
[11]. Xinshu Niu, Weiping Du, Weimin Du, Sens. Actuators B 99 (2004) 405–409.
[12]. S. L. Darshane,, R. G. Deshmukh, S. S. Suryavanshi, I. S. Mulla J. Am. Ceram. Soc., 91 (2008) 2724–2726.
[13]. D. R. Patil, L. A. Patil, Room temperature chlorine gas sensing using surface modified ZnO thick film resistors, Sens. Actuators B 123 (2007) 546-553.
[14]. L. A. Patil, D. R. Patil, Heterocontact type CuO-modified SnO_2 sensor for the detection of a ppm level H_2S gas at room temperature, Sens. Actuators B 120 (2006) 316-323.
[15]. D. R. Patil, L. A. Patil, Preparation and study of NH_3 gas sensing behavior of Fe_2O_3 doped ZnO thick film resistors, Sens. Transducers 70 (2006) 661-670.
[16]. D. R. Patil, L. A. Patil, P. P. Patil, Cr_2O_3-activated ZnO thick film resistors for ammonia gas sensing operable at room temperature, Sens. Actuators B 126 (2007) 368–374.
[17]. D. R. Patil, L. A. Patil, Ammonia sensing resistors based on Fe_2O_3-modified ZnO thick films, Sensors IEEE 7 (2007) 434-439.
[18]. D. R. Patil, L. A. Patil, Al_2O_3-modified ZnO based thick film resistors for H_2-gas sensing, Sens. Transducers 81 (2007) 1354-1363.
[19]. K. M. Garadkar, B. S. Shirke, P. P. Hankare, D. R. Patil, Low cost nanostructured anatase TiO_2 as a H_2S Gas sensor synthesized by microwave assisted technique, Sensor Letters 9 (2010) 526 – 532.
[20]. L. Satyanarayana, K. M. Reddey, S. V. Manorama, Sens. Actuators B 89 (2003) 62.
[21]. A. Ratna Phani, S. Manorama, V. J. Rao, Appl. Phys. Lett. 66, (1995) 2619.
[22]. Duk-Dong Lee, Dae-Sik Lee, IEEE Sensors 1 (2001) 214.
[23]. O. V. Safonova, G. Delabonglise, B. Chenevier, A. M. Gaskov, M. Labeau, J. Mater. Sci. Engg. C 21 (2002) 105.
[24]. C. Bittencourt, E. Lobet, M. A. P. Silva, R. Lauders, L. Nieto, K. O. Vicaro, J. E. Sueiras, J. Calderer, X. Correig, Sens. Actuators B 1 (2003) 6992.
[25]. N. Iftimie, E. Rezlescu, P. D. Popa, N. Rezlescu J. Optoelectronics and Advanced Materials 7 (2005) 911.
[26]. L. A. Patil and D. R. Patil , Sens. Actuators B, 120, (2006) 316-323.
[27]. Cui-Ping Liu, Ming-Wei Li, Zhong Cui, Juan-Ru Huang, Yi-Ling Tian, Tong Lin and Wen-Bo Mi, J. Mater. Sci., 42 (2007) 6133.
[28]. A.K. Verma, T.C. Goal, J. Magn. Magn. Mater., 192 (1999) 271.
[29]. U. B. Gawas, V. M. S. Verenkar, D. R. Patil, Nanostructured ferrite based electronic nose sensitive to ammonia at room temperature, Sens. Transducers 134 (2011) 45-55.
[30]. S. V. Bangale, S. M. Khetre, D. R. Patil, S. R. Bamne, Simple synthesis of $ZnCo_2O_4$ nanoparticles as gas sensing materials, Sens. Transducers 134 (2011) 95-106.
[31]. S. V. Bangale, D. R. Patil, S. R. Bamne, Nanostructured spinel $ZnFe_2O_4$ for the detection of chlorine gas, Sens. Transducers 134 (2011) 107-119.
[32]. S. V. Bangale, D. R. Patil, S. R. Bamne, Preparation and electrical properties of nanocrystalline $MgFe_2O_4$ oxide by combustion route, Arch. Appl. Sci. Res. 3 (5) (2011) 506 – 513.
[33]. D. R. Patil, Need of gas sensors, J. Everyman's Science, 46 (2011) 155 – 161.
[34]. S. D. Kapse, F. C. Raghuwanshi, V. D. Kapse, D. R. Patil, Characteristics of high sensitivity ethanol gas sensors based on nanostructured spinel $Zn_{1-x}Co_xAl_2O_4$, J. Current Appl. Phys. 12 (2012) 307 – 312.
[35]. K. A. Khamkar, S. V. Bangale, V. V. Dhapte, D. R. Patil, S. R. Bamne, A Novel Combustion Route for the Preparation of Nanocrystalline $LaAlO_3$ Oxide Based Electronic Nose Sensitive to NH_3 at Room Temperature, Sens. Transducers 146 (2012) pp. 145-155.
[36]. P. P. Hankare, K. R. Sanadi, K. M. Garadkar, D. R. Patil, I. S. Mulla, Synthesis and characterization of nickel substituted cobalt ferrite nanoparticles by sol-gel auto-combustion method, J. Alloys and Compounds 553 (2013) pp 383-388.